

This discussion paper is/has been under review for the journal *Climate of the Past* (CP).  
Please refer to the corresponding final paper in CP if available.

## Climate and vegetation changes around the Atlantic Ocean

D. Handiani et al.

# Climate and vegetation changes around the Atlantic Ocean resulting from changes in the meridional overturning circulation during deglaciation

D. Handiani<sup>1</sup>, A. Paul<sup>1,2</sup>, and L. Dupont<sup>2</sup>

<sup>1</sup>Department of Geosciences, University of Bremen, Bremen, Germany

<sup>2</sup>MARUM – Center for Marine Environmental Sciences, University of Bremen, Bremen, Germany

Received: 19 June 2012 – Accepted: 11 July 2012 – Published: 24 July 2012

Correspondence to: D. Handiani (dhandiani@marum.de)

Published by Copernicus Publications on behalf of the European Geosciences Union.

Title Page

Abstract

Introduction

Conclusions

References

Tables

Figures

⏪

⏩

◀

▶

Back

Close

Full Screen / Esc

Printer-friendly Version

Interactive Discussion

## Abstract

The Bølling-Allerød (BA, starting ~ 14.5 ka BP) is one of the most pronounced abrupt warming periods recorded in ice and pollen proxies. The leading explanation of the cause of this warming is a sudden increase in the rate of deepwater formation in the North Atlantic Ocean and the resulting effect on the heat transport by the Atlantic Meridional Overturning Circulation (AMOC). In this study, we used the University of Victoria (UVic) Earth System-Climate Model (ESCM) to run simulations, in which a freshwater perturbation initiated a BA-like warming period. We found that under present climate conditions, the AMOC intensified when freshwater was added to the Southern Ocean. However, under Heinrich event 1 (HE1, ~ 16 ka BP) climate conditions, the AMOC only intensified when freshwater was extracted from the North Atlantic Ocean, possibly corresponding to an increase in evaporation or a decrease in precipitation in this region. The intensified AMOC led to a warming in the North Atlantic Ocean and a cooling in the South Atlantic Ocean, resembling the bipolar seesaw pattern typical of the last glacial period.

In addition to the physical response, we also studied the simulated vegetation response around the Atlantic Ocean region. Corresponding with the bipolar seesaw hypothesis, the rainbelt associated with the Intertropical Convergence Zone (ITCZ) shifted northward and affected the vegetation pattern in the tropics. The most sensitive vegetation area was found in tropical Africa, where grass cover increased and tree cover decreased under dry climate conditions. An equal but opposite response to the collapse and recovery of the AMOC implied that the change in vegetation cover was transient and robust to an abrupt climate change such as during the BA period, which is also supported by paleovegetation data. The results are in agreement with paleovegetation records from Western tropical Africa, which also show a reduction in forest cover during this time period. Further agreement between data and model results was found for the uplands of North America and Southern Europe, where grassland along with warm and dry climates were simulated. However, our model simulated vegetation

## Climate and vegetation changes around the Atlantic Ocean

D. Handiani et al.

Title Page

Abstract

Introduction

Conclusions

References

Tables

Figures



Back

Close

Full Screen / Esc

Printer-friendly Version

Interactive Discussion



changes in South and North America that were much smaller than reconstructed. Along the west and east coast of North America we simulated drier vegetation than the pollen records suggest.

## 1 Introduction

5 After the cooling associated with Heinrich Event 1 (HE1), an abrupt warming of the surface climate at the onset of the Bølling-Allerød period (BA) has been recorded in the North Atlantic Ocean (e.g. Bard et al., 2000; McManus et al., 2004), concurrent with climate changes in the South Atlantic Ocean (e.g. EPICA members, 2006; Barker et al., 2009; Stenni et al., 2011). The climate changes in the two hemispheres follow  
10 the pattern of a bipolar seesaw typical of the last glacial period (Stocker and Johnsen, 2003). They are connected to the strengthening of the Atlantic Meridional Overturning Circulation (AMOC) through heat transport driven by two deepwater sources: the North Atlantic Deep Water (NADW) in the Northern Hemisphere, and the Antarctic Bot-  
15 tom Water (AABW) in the Southern Hemisphere (e.g. Broecker, 1998; Stocker, 1998; Stocker et al., 2001). Sea-level reconstructions suggest that the AMOC recovery mechanism is associated with meltwater flux causing the sea-level to rise by several meters within a century (Fairbanks, 1989; Bard et al., 1990, 2010; Clark et al., 2002; Siddall et al., 2004), although the exact timing and meltwater sources are a matter of current debate (e.g. Peltier et al., 2006; Driesschaert et al., 2007; Stanford et al., 2006).

20 Model studies have been performed that simulate the recovery of the AMOC after its collapse invoking different mechanisms. The most successful of these are (1) a reduction of the meltwater flux into the North Atlantic Ocean (Ganopolski and Rahmstorf, 2001), (2) negative freshwater forcing of the North Atlantic Ocean (Schmittner et al., 2002b), (3) an additional meltwater flux into the Southern Ocean (Weaver et al., 2003),  
25 and (4) warming and sea-ice retreat in the Southern Ocean (Knorr and Lohmann, 2007). Recently, transient model simulations suggest that the large abrupt warming at the onset of the BA period is the result of several overlapping climate responses

## Climate and vegetation changes around the Atlantic Ocean

D. Handiani et al.

Title Page

Abstract

Introduction

Conclusions

References

Tables

Figures



Back

Close

Full Screen / Esc

Printer-friendly Version

Interactive Discussion



such as an increase of atmospheric CO<sub>2</sub>, the AMOC recovery after HE1, and an overshoot of the AMOC after gradual forcing of the meltwater flux (Liu et al., 2009). In our study, we focus on the effect of the abrupt warming on the vegetation cover during the Late Glacial, with an emphasis on vegetation changes between the HE1 stadial and the BA interstadial as well as the glacial state before HE1.

The pollen assemblage studies in the Atlantic Ocean region indeed show profound changes in the vegetation cover during the BA period. As an example, in West and Southwest North America a boreal or warm temperate forest became dominant about 15 ka BP (ka BP = thousands years before present), indicating a warm and wet climate concurrent with the abrupt warming event in Greenland during the final stages of the last glacial period (Jiménez-Moreno et al., 2010). During the same time, much of Europe was covered by warm temperate forest, also corresponding to a relatively warm and humid climate (Fletcher et al., 2010). The pattern of vegetation change in tropical Africa and tropical South America was more complex (Hessler et al., 2010), e.g., the Northeastern Brazilian record indicates the occurrence of Atlantic forest and a humid climate during the last phase of HE1, followed by a decline in forest and increase in aridity. In contrast, pollen records from West Africa (Angola and Southern Congo) show no clear trend during the BA period, while in East Equatorial Africa temperate-montane forest and tropical forest developed when the climate got warmer after HE1.

With these records as a reference, we carried out experiments with a numerical model in an attempt to initiate the recovery of the AMOC after its collapse and simulate the BA warming following HE1. Our experiments were inspired by the simulations of Weaver et al. (2003), who trigger the onset of the BA period by adding freshwater to the South Atlantic Ocean. We used the same Earth System Model of Intermediate Complexity (EMIC) – the University of Victoria Earth System-Climate Model (UVic ESCM) – complemented with a dynamic global vegetation model (Meissner et al., 2003), which enabled us to study the interaction between climate and vegetation during the recovery of the AMOC.

## Climate and vegetation changes around the Atlantic Ocean

D. Handiani et al.

Title Page

Abstract

Introduction

Conclusions

References

Tables

Figures



Back

Close

Full Screen / Esc

Printer-friendly Version

Interactive Discussion



## Climate and vegetation changes around the Atlantic Ocean

D. Handiani et al.

Title Page

Abstract

Introduction

Conclusions

References

Tables

Figures

⏪

⏩

◀

▶

Back

Close

Full Screen / Esc

Printer-friendly Version

Interactive Discussion



In addition, we also present a preliminary comparison between the model results and pollen records during the onset of the BA warm period using a biome distribution generated from our model output in order to simplify the data-model comparison (Handiani et al., 2012). Thus our study aims to understand the vegetation development at the onset of the BA period and tries to elucidate the interactions between climate and land-cover during periods of abrupt climate change.

## 2 Model description and experimental designs

The UVic ESCM version 2.8 (Weaver et al., 2001) consists of a three-dimensional ocean model (MOM – Modular Ocean Model version 2) (Pacanowski, 1995), a vertically integrated two-dimensional energy-moisture balance model of the atmosphere (Fanning and Weaver, 1996), and a dynamic-thermodynamic sea-ice model (Hibler, 1979; Hunke and Dukowicz, 1997; Bitz et al., 2001). This version further includes an adaptation of the land surface model MOSES2 (Met Office Surface Exchange System version 2) (Cox et al., 1999) and the dynamic global vegetation model (DGVM) TRIFFID (Top-down Representation of Interactive Foliage and Flora Including Dynamics) (Cox, 2001; Meissner et al., 2003). It also includes a fully coupled carbon cycle, which takes into account the terrestrial carbon fluxes and pools (Meissner et al., 2003; Matthews et al., 2005), as well as the inorganic and organic carbon in the ocean (Ewen et al., 2004; Schmittner et al., 2007). However, our simulations did not include the ocean carbon cycle component.

The coupled climate model is forced by seasonal variations of insolation, wind stress at the ocean surface and land-ice cover. Here we used the global ice sheet reconstruction ICE-5G (Peltier, 2004) for the present day as well as the Last Glacial Maximum (LGM). The TRIFFID model simulates the plant distribution based on carbon fluxes between land and atmosphere. This carbon flux is represented by the structure and coverage of five Plant Functional Types (PFTs) and soil carbon storage. The PFTs are

broadleaf and needleleaf trees, C<sub>3</sub> and C<sub>4</sub> grasses, and shrubs. All models used the same horizontal grid resolution of 1.8° latitude by 3.6° longitude.

We carried out three sequences of experiments, each with a similar design except for different forcing and boundary conditions (Table 1). The boundary conditions were taken to represent the climate conditions of the present day (PI), LGM (21 ka BP) and HE1 (16 ka BP). Each sequence covered 4500 simulated years. First, the model was spun up for 2000 yr. After reaching the equilibrium state, Heinrich climate-like conditions were simulated by increasing the freshwater discharge into the North Atlantic Ocean (region A, Fig. 1a) linearly from 0 to 0.2 Sv (1 Sv = 10<sup>6</sup> m<sup>3</sup> s<sup>-1</sup>) over a period of 1000 simulated years. As shown by Weaver et al. (2003), this amount of freshwater perturbation is enough to slow down or terminate the deep-water formation in the UVic ESCM. We tried to re-establish the AMOC after its collapse by adding freshwater to a region west of West Antarctica (region B, Fig. 1a) at a rate increasing from 0 to 1 Sv over a period of 500 yr. This site was chosen because it is a potential location for freshwater discharge from the melting continental ice sheet and might have played a role in the recovery of the AMOC (Clark et al., 1996; Kanfoush et al., 2000; Weaver et al., 2003) as well as a place of the Antarctic Intermediate Water (AAIW) formation. The final 1000 yr of simulation was run without any freshwater perturbation (Fig. 2).

Furthermore, we ran an additional simulation with HE1 boundary conditions, called H1\_EXT (Table 1), in which we applied a strong negative freshwater flux anomaly at a constant rate of -0.3 Sv over a period of 500 yr to the North Atlantic Ocean (region C), which is another possible way of triggering the recovery of the AMOC after its collapse (e.g. Schmittner et al., 2002b). The conditions for the remainder of this simulation were the same as for the final 1000 yr of all sequences. Finally, we compared the model result of the H1\_EXT experiment with pollen records from the region around the Atlantic Ocean compiled in terms of biomes (Fig. 1, Table 2). To facilitate this data-model comparison, the results from the DGVM were translated into biomes using the algorithm described by Handiani et al. (2012). This algorithm combines the potential

## Climate and vegetation changes around the Atlantic Ocean

D. Handiani et al.

Title Page

Abstract

Introduction

Conclusions

References

Tables

Figures

⏪

⏩

◀

▶

Back

Close

Full Screen / Esc

Printer-friendly Version

Interactive Discussion



PFTs calculated by the DGVM and environmental constraints such as temperature and the number of growing degree days.

### 3 Results

#### 3.1 The variability of AMOC and physical ocean properties

5 The model produced different deep-water formation histories for the three different sequences of simulations, initialized from three different climate states (present day, last glacial maximum, and pre-Heinrich event 1; denoted hereafter PI, GL, H1, respectively; cf. Table 1). The strongest and deepest AMOC was established in the PI simulation, while the lowest and shallowest developed in the GL simulation. The maximum of the AMOC streamfunction reached 21 Sv, 10 Sv, and 16 Sv in the PI, LGM, and H1 sequences, respectively (Fig. 2). In all simulation sequences, the AMOC collapsed after perturbing the freshwater balance in region A, while they performed differently when the freshwater was added to region B. In the PI sequence, the maximum of the AMOC streamfunction increased from 1 Sv at the end of the freshwater perturbation in region A to 13 Sv at the end of the perturbation in region B ( $T_1$  in Fig. 2), and it continued to increase up to 21 Sv. In the H1 sequence, the maximum of the streamfunction increased from 1 Sv to only 2 Sv at the end of the freshwater perturbation in region B and then returned to collapsed conditions until the end of the sequence (Fig. 2). However, in the H1\_EXT sequence, the AMOC recovered, and the maximum of the streamfunction experienced an overshoot occurring a few decades after the negative freshwater input to region C ceased. The maximum of the AMOC streamfunction increased quite sharply to 30 Sv, then decreased to 16 Sv after a few hundred years, where it remained until the end of the simulation ( $T_2$  in Fig. 2). In contrast, in the GL sequence the maximum of the streamfunction remained unchanged for 500 yr after adding freshwater to region B, and the AMOC stayed in a collapsed state until the end (Fig. 2).

## Climate and vegetation changes around the Atlantic Ocean

D. Handiani et al.

Title Page

Abstract

Introduction

Conclusions

References

Tables

Figures

⏪

⏩

◀

▶

Back

Close

Full Screen / Esc

Printer-friendly Version

Interactive Discussion



## Climate and vegetation changes around the Atlantic Ocean

D. Handiani et al.

Title Page

Abstract

Introduction

Conclusions

References

Tables

Figures



Back

Close

Full Screen / Esc

Printer-friendly Version

Interactive Discussion



The relative abundance of the two major water masses involved in the AMOC, NADW and AABW, is determined by their density. When the density of one water mass increases relatively to the other, it will occupy a larger fraction of the volume of the Atlantic Ocean (Stocker et al., 1992; Schmittner et al., 2002a). Zonally averaged density anomalies in the Atlantic Ocean (Fig. 3) show the differences between simulated conditions 500 yr after adding freshwater to region B ( $T_1$  in Fig. 2) and the collapse triggered by perturbing region A ( $T_0$  in Fig. 2). Furthermore, the individual contributions of temperature and salinity to the density anomalies are indicated. In all sequences, salinity is the dominant component in the total density anomaly after 500 yr of adding freshwater to region B. The AAIW freshened significantly in the PI and H1 sequences at time  $T_1$  (Fig. 3c, i). In contrast, the AAIW did not show any change in the GL sequence after the freshwater perturbation in region B (Fig. 3f). Furthermore, the fate of NADW was different in the three different simulation sequences: it became denser in PI, lighter in H1, and even disappeared in GL. The density anomaly in the H1\_EXT simulation (Fig. 3j–l) is somewhat similar to that in the PI sequence with freshwater perturbation in region B (Fig. 3a–c), but the AAIW became fresher and the NADW denser after 500 yr of extracting freshwater from the North Atlantic Ocean.

The changes in AMOC strength are better understood in terms of the zonally averaged depth-integrated steric height. We calculated the steric height following Schmittner et al. (2002a), and compared the results at times  $T_1$  and  $T_0$  (Fig. 2). The total steric height gradient ( $\Delta\phi$ ) is shown together with contributions due to temperature ( $\Delta\phi_T$ ) and salinity ( $\Delta\phi_S$ ) changes for each simulation (Fig. 4). As suggested by earlier studies (Hughes and Weaver, 1994; Wiebe and Weaver, 1999; Schmittner et al., 2002a), the steric height gradient between the southern tip of Africa ( $35^\circ$  S), where the eastern zonal boundary of the Atlantic Ocean ends, and the regions of deep water formation around  $60^\circ$  N is proportional to the strength of the AMOC formation.

The steric height gradient between the latitudes of  $35^\circ$  S and  $60^\circ$  N in the PI sequence at  $T_1$  decreased with respect to the simulation at  $T_0$  (Fig. 4a) due to the intensified AMOC after the freshwater perturbation in region B (Fig. 1a). This was consistent with

the dominance of the salinity component within the decreased steric height anomaly (Fig. 4a). A small change of the difference in density in the GL sequence between  $T_1$  and  $T_0$  (Fig. 3d) was consistent with small changes in the steric height gradient between  $35^\circ$  S and  $60^\circ$  N and the AMOC in these simulations (Fig. 4b). The temperature and salinity contributions to the change in the steric height gradient were also small. The difference in the steric height gradient in the H1 sequence between times  $T_1$  and  $T_0$  was also small, except that in this case the salinity and temperature contributions showed appreciable but opposite changes between  $35^\circ$  S and  $35^\circ$  N (Fig. 4c). The anomaly pattern in the steric height gradient between times  $T_1$  and  $T_0$  in the H1\_EXT sequence (Fig. 4d) was similar to that of the PI sequence (Fig. 4a), except that the differences in the temperature and salinity contributions were larger in the H1\_EXT than in the PI sequence. Both anomalies resulted in a recovery of the AMOC, although in different ways.

Differences in sea-surface temperature (SST) between the collapsed state ( $T_0$ , after adding freshwater to region A) and the partial recovery of the AMOC ( $T_1$ , after 500 yr of adding freshwater to region B or extracting freshwater from region C) for the PI, GL, H1 and H1\_EXT sequences are given in Fig. 5a–d. For the PI sequence, the temperature decreased both in the North and South Atlantic Ocean. For the GL sequence, it hardly changed or showed only a slight warming in the Southern North Atlantic Ocean. In the case of the H1 and H1\_EXT sequences, the SST increased in the North Atlantic Ocean and decreased in the South Atlantic Ocean, whereby the anomalies were bigger in the North Atlantic Ocean after extracting freshwater from region C in the North Atlantic Ocean (H1\_EXT) than after adding freshwater to region B near Antarctica (H1). The mean anomalies in SST in the North Atlantic Ocean ( $0^\circ$ – $100^\circ$  W and  $25^\circ$ – $70^\circ$  N) were  $-0.85^\circ\text{C}$  for the PI and  $0.26^\circ\text{C}$  for the H1 sequence, respectively. For comparison, in the South Atlantic Ocean ( $20^\circ$  E– $73^\circ$  W and  $25^\circ$ – $70^\circ$  S), the mean anomalies were  $-1.52^\circ\text{C}$  for the PI and  $-0.78^\circ\text{C}$  for the H1 sequence. The mean SST anomalies in the GL sequence were slightly smaller,  $-0.17^\circ\text{C}$  in the North Atlantic Ocean and  $-0.11^\circ\text{C}$  in the South Atlantic Ocean. The SST anomalies show that adding freshwater

## Climate and vegetation changes around the Atlantic Ocean

D. Handiani et al.

[Title Page](#)[Abstract](#)[Introduction](#)[Conclusions](#)[References](#)[Tables](#)[Figures](#)[⏪](#)[⏩](#)[◀](#)[▶](#)[Back](#)[Close](#)[Full Screen / Esc](#)[Printer-friendly Version](#)[Interactive Discussion](#)

to region B led to a warming in the North Atlantic Ocean, although the AMOC did not necessarily recover (Fig. 2).

### 3.2 Precipitation and vegetation response

Precipitation was generally higher over the North Atlantic Ocean than over the South Atlantic Ocean for all simulation sequences (Fig. 5e–h). This was due to a northward shift of the region of high tropical precipitation, associated with the ITCZ. A warmer SST in the North Atlantic Ocean was accompanied by significantly increased precipitation from 0° to 30° N and reduced precipitation from 0° to 30° S. Over land, the anomaly pattern was similar in all simulations. The Western Sahara showed the largest anomaly of the Northern Hemisphere. Northeast Brazil and Southwestern Africa became drier compared with other parts of the Southern Hemisphere. An interesting feature occurred in the simulation initialized from the PI sequence (Fig. 5e), in which precipitation increased between 15° and 30° N and decreased between 15° N to 30° S. This precipitation pattern was stronger compared to that of the other sequences.

Generally, the vegetation response at time  $T_1$  compared to time  $T_0$  was relatively minor in all sequences (Fig. 6). Relatively strong responses occurred in Western South America, Southern Europe, Northwest Eurasia, and in Africa (Sahara and Sahel). This was connected with the substantial precipitation changes in those areas. For example, in the PI sequence, precipitation strongly increased in the Western Sahara, corresponding to an increase in grasses (Fig. 6e). Like the precipitation pattern (Fig. 5a–h), the vegetation response in the PI sequence (Fig. 6a, e) differed considerably from the other simulated sequences (Fig. 6b–d and f–h). Significant changes occurred in tropical Africa and Northern South America, as well as in the mid- to high latitudes. Trees and grasses sharply decreased in the Eastern Sahel region, while only trees decreased in Western South America (Fig. 6a, e). In contrast, a sharp increase in grasses occurred in Northwest Africa. This feature was also found in the H1\_EXT simulation (Fig. 6h), which developed a strength of the AMOC similar to that of the PI simulation 500 yr after extracting freshwater from region C or adding freshwater to region B ( $\sim 13$  Sv),

## Climate and vegetation changes around the Atlantic Ocean

D. Handiani et al.

Title Page

Abstract

Introduction

Conclusions

References

Tables

Figures



Back

Close

Full Screen / Esc

Printer-friendly Version

Interactive Discussion



respectively. Furthermore, in the GL and H1 sequences, vegetation cover remained relatively unchanged, whereas tree and grass cover after 500 yr of the freshwater perturbation in region B remained similar to those at the end of the freshwater perturbation in region A (Fig. 6b, c, f and g). However, an exception occurred in the H1 sequence (Fig. 6c, g), where trees decreased sharply (~ 60 %) and grasses increased in the center of the Sahel.

Distinct changes of vegetation occurred in the mid- to high latitudes around the North Atlantic Ocean (e.g., in North America, Europe, and Western Russia) in the PI and H1\_EXT sequences. In the PI sequence, trees strongly decreased in Eastern North America while grasses increased. In Western Europe, grasses decreased by ~ 60 %, while trees increased by 20 % (Fig. 6a, e). A unique feature occurred in Eastern North America where grasses increased by 80 % in the PI sequence and decreased in all other sequences. The magnitude by which grasses decreased varied, however. The largest decrease (of ~ 40 %) was in the GL sequence (Fig. 6f). In Eastern Europe (around present-day Ukraine), grasses increased substantially in all sequences. The biggest increase was in the PI sequence by ~ 70 % (Fig. 6e), while in the other sequences it increased by ~ 20–60 % (Fig. 6f, g, h).

To understand the vegetation differences between the climate conditions before and after the AMOC recovery, we compared the tree and grass cover at times  $T_2$  and  $T_{-1}$  between 110° W and 60° E longitude and between 50° S and 70° N latitude (Fig. 7). There was relatively little vegetation change between these two climate conditions in the PI and HE1\_EXT sequences, except for some slight changes in the Northern Hemisphere (from the equator to 60° N) and in Southern South America (around 20° S). The total changes in trees or grasses were less than 10 % (Fig. 7a, d). The tree and grass cover changes of the GL and H1 sequences were substantial and followed similar trends, although the magnitude of the changes were slightly smaller in the H1 sequence (Fig. 7c). At the end of both sequences, grass cover decreased between 20° N and 50° N, the maximum increase of grasses (with differences up to 40 %) occurred at 60° N, and tree cover declined near 20° N (Fig. 7b, c).

## Climate and vegetation changes around the Atlantic Ocean

D. Handiani et al.

[Title Page](#)[Abstract](#)[Introduction](#)[Conclusions](#)[References](#)[Tables](#)[Figures](#)[⏪](#)[⏩](#)[◀](#)[▶](#)[Back](#)[Close](#)[Full Screen / Esc](#)[Printer-friendly Version](#)[Interactive Discussion](#)

### 3.3 Comparison between model and paleovegetation data

Pollen studies for the BA period show mostly grassland and temperate forest in Western and Southeast North America, as well as in Southern Europe, although warm temperate and boreal forest also occurred in Western North America. Tropical Africa and South America were covered by savanna and warm temperate forest (Fig. 1b, Table 2).

The reconstructed biomes of our model simulations showed a pattern at time  $T_1$  similar to that of the proxy reconstructions for the beginning of the BA period, albeit a few differences exist (Fig. 8). In the PI sequence, grass cover dominated in Eastern Europe and North America, while boreal forest was found in Europe and Central America. In this sequence, the tropics were mainly covered by tropical forest except for small regions of savannah found in Western South America and Africa (Fig. 8a). The biome patterns in Southeastern North America, Europe, and South America were similar in all sequences, except in the extent of the area covered. The GL sequence was the most different. For example, temperate forest in Eastern Europe (Ukraine) covered the smallest area in the GL sequence (Fig. 8b). Warm temperate forest in Southeast North America occupied the same small area in all sequences, except for the GL sequence, where forest cover was simulated along the North and South Carolina coastline (compare Fig. 8b with 8a, c, d).

The model results and paleovegetation data of grass covered regions in Western North America, Southern Europe, and the Mediterranean are in good agreement (compare Figs. 8 and 1). The savanna and warm temperate forest in Southeast Africa in the model output is supported by paleo-records. Temperate forest in Southeast North America was not simulated by the model, in which grassland and warm temperate forest dominated (Fig. 8d). Model and paleovegetation data disagree in Northeast and Southeast Brazil as well as in Western tropical South America. The model output indicates tropical forest in these regions, while pollen records suggest a warm temperate forest in tropical Western South America and Northeast Brazil, and savanna grassland in Southeast Brazil.

## Climate and vegetation changes around the Atlantic Ocean

D. Handiani et al.

Title Page

Abstract

Introduction

Conclusions

References

Tables

Figures



Back

Close

Full Screen / Esc

Printer-friendly Version

Interactive Discussion



## 4 Discussion

Whether, or to what degree, deepwater formation in the North Atlantic Ocean during the last deglaciation is controlled by perturbing the freshwater balance of the Southern Ocean is still under debate (Trevena et al., 2008; Swingedouw et al., 2009). We note that in all simulation sequences the North Atlantic Ocean warmed relative to the South Atlantic Ocean after freshwater was added in the Southern Hemisphere, although the AMOC strength did only recover in one out of three simulations. The AMOC strength recovered only in the PI sequence that used present-day orbital parameters and CO<sub>2</sub> concentration. This result was similar to that of Weaver et al. (2003) who point out that there is a strong interhemispheric link between global-scale water masses distribution and the thermohaline circulation. By applying a freshwater perturbation in the area of AAIW formation, the density of AAIW decreases and, in turn, the density of NADW relatively increases, inducing a gradual intensification of the AMOC.

In contrast, adding freshwater in the Southern Hemisphere did not lead to a recovery of the AMOC strength under GL and H1 sequences. Either the AMOC remained in a collapsed state, or it temporally intensified, albeit only slightly. The surface of the North Atlantic Ocean slightly warmed, became slightly more saline and overall became less dense. At greater depths, density did not change in the GL sequence and slightly decreased in the H1 sequence. Slightly reduced density of deep waters in the H1 sequence was mainly due to the freshwater perturbation applied to region B in the Southern Hemisphere. This suggests that perturbing the freshwater balance in the Southern Hemisphere to form denser AAIW is not guaranteed to drive the deep overturning circulation from a collapsed state back to an active state at its initial strength. This is probably because the density contrast between the North and South Atlantic Oceans has less impact on the strength of the AMOC strength when the NADW is already fresher and shallower (as it was in the case of the GL and H1 sequences). Furthermore, when the freshwater balance in the Northern Hemisphere was perturbed, the collapse of the AMOC was faster under LGM and HE1 than under present day

### Climate and vegetation changes around the Atlantic Ocean

D. Handiani et al.

Title Page

Abstract

Introduction

Conclusions

References

Tables

Figures



Back

Close

Full Screen / Esc

Printer-friendly Version

Interactive Discussion



background climate conditions. Our simulations thus support that the glacial AMOC is more vulnerable to a perturbation of the freshwater balance of the North Atlantic Ocean and less susceptible to a recovery of the AMOC by a perturbation of the freshwater balance in the Southern Ocean (e.g. Ganopolski and Rahmstorf, 2001; Schmittner et al., 2002a; Trevena et al., 2008; Kageyama et al., 2009).

Salinity played an important role in the AMOC recovery mechanism. This is indicated by the salinity contribution to the density anomalies in the PI and H1\_EXT sequences, which showed a similar pattern after the AMOC recovered. The pattern was different from the one seen in the GL and H1 sequences, although the temperature component of the density anomalies contributed to warming at time  $T_1$  in all sequences. The salinity component of the density anomalies in the PI and H1\_EXT sequences contributed to saltier waters, foremost in the North Atlantic Ocean. On the other hand, in the GL and particularly the H1 sequences, the deep water became less saline.

Stouffer et al. (2006) use an atmosphere-ocean general circulation (AOGCM) to investigate the response to freshwater perturbations in the North Atlantic Ocean ( $50^{\circ}$ – $70^{\circ}$  S) and the Southern Ocean (south of  $60^{\circ}$  S). They suggest that the AMOC is mainly unchanged in the case of the freshwater perturbation near Antarctica, although a slight weakening of the AMOC is seen at the end of their simulation, for which they propose two mechanisms: firstly, the reduced contrast of sea surface salinity (SSS) between the North Atlantic and the North Pacific Oceans and, secondly, freshwater from the Southern Hemisphere reaching far into the North Atlantic Ocean hindering the sinking of surface waters at high latitudes, which leads to a reduced AMOC. These mechanisms are also found in our simulations. When the effect of the freshwater perturbation west of West Antarctica reaches the North Atlantic Ocean, it is responsible for SSS changes and hinders the sinking of surface waters, thus influencing the AMOC.

Weber et al. (2007) compare the response of the AMOC to LGM boundary conditions in nine Paleoclimate Modeling Intercomparison Project (PMIP) models with respect to three mechanism: changes in net evaporation over the Atlantic basin, local processes within the Atlantic basin as expressed by the density difference between its northern

## Climate and vegetation changes around the Atlantic Ocean

D. Handiani et al.

Title Page

Abstract

Introduction

Conclusions

References

Tables

Figures

⏪

⏩

◀

▶

Back

Close

Full Screen / Esc

Printer-friendly Version

Interactive Discussion



and southern ends, and the deep overturning cell associated with the formation of AABW in the Southern Ocean. For two EMICs, the UVic ESCM and the ECBilt-CLIO (de Vries and Weber, 2005), they cannot identify the process that dominates the AMOC response. In a subsequent study, however, Weber and Drijfhout (2007) determine for the ECBilt-CLIO that under LGM climate conditions the AMOC remains in a collapsed state after a freshwater perturbation as long as the initial AMOC transports freshwater out of the Atlantic basin. Furthermore, they find that the AMOC recovers when the AMOC transports freshwater into the Atlantic basin. Similarly, in our glacial simulations (GL and H1), the freshwater transport by the initial AMOC at the southern boundary was into the Atlantic basin (northward), and both our simulations remained in a collapsed state after a freshwater perturbation was applied to the North Atlantic Ocean. The AMOC intensified under preindustrial boundary conditions with a northward overturning freshwater transport at the southern boundary of the Atlantic basin.

The H1\_EXT sequence – which applied extraction of freshwater from the North Atlantic Ocean (e.g. Manabe and Stouffer, 1997; Schmittner et al., 2002b) – succeeded in recovering the AMOC. The density profile in the North Atlantic Ocean after the extraction of freshwater indicated warmer and saltier surface waters and denser and cooler waters at the depth of the NADW. This density profile was similar to that of the PI sequence, except that the salinity and temperature components were stronger than in the PI sequence. The negative freshwater flux applied in the H1\_EXT sequence may correspond to reduced precipitation, enhanced evaporation or reduced runoff and melting. The effect of freshwater extraction has been investigated in detail in an earlier version of the UVic model by Schmittner et al. (2002b), who reviewed the feedbacks between the Atlantic overturning and the ice sheet mass balance. They proposed the mechanism of growing ice sheet volume in response to the transition from a stadial to an interstadial during the LGM climate. Schmittner et al. (2002b) started their simulation with a linear decrease of freshwater in the North Atlantic Ocean and continued forcing with a constant negative freshwater perturbation until the end of the simulation. In one of their cases, the interstadial was stable and led to a constant increase of the

## Climate and vegetation changes around the Atlantic Ocean

D. Handiani et al.

Title Page

Abstract

Introduction

Conclusions

References

Tables

Figures



Back

Close

Full Screen / Esc

Printer-friendly Version

Interactive Discussion



North Atlantic salinities, which allowed recovery of the AMOC. Using a transient simulation with the coupled atmosphere-ocean general circulation model (AOGCM) of the National Center for Atmospheric Research (NCAR) Community Climate System Model version 3 (CCSM3), Liu et al. (2009) suggest that the abrupt warming at the onset of the BA may not be caused by freshwater forcing alone, but by overlapping climatic responses to increasing atmospheric CO<sub>2</sub> concentrations, the recovery of the AMOC after the HE1 period, and an AMOC overshoot.

In order to examine the effects of changing CO<sub>2</sub> concentrations in the UVic ESCM, preliminary investigations with transient CO<sub>2</sub> for different initial climate conditions have been performed by Weaver et al. (2007). They find that the AMOC declines in all their experiments and that the largest decline is in the experiment with the strongest initial value of the AMOC. However, they also find that all experiments in which the initial atmospheric CO<sub>2</sub> concentration is 240 ppm or below and the initial AMOC strength less than 17.4 Sv, the freshwater fluxes act to strengthen the AMOC. In contrast, the freshwater flux acts to weaken the AMOC in an experiment with a CO<sub>2</sub> concentration exceeding 240 ppm. Thus the dominance of heat flux over freshwater flux changes as a cause of the AMOC weakening appears to depend on the initial climate state. This result argues in favor of performing similar simulations using glacial boundary conditions to examine climate and AMOC changes at the onset of the BA period.

The warm climate in the North Atlantic Ocean, which possibly results from the recovery of the AMOC after its collapse (e.g. Boyle and Keigwin, 1987; McManus et al., 2004), may also be linked to changes in tropical precipitation and vegetation. During the abrupt warming in the H1\_EXT sequence, vegetation showed no response in tropical South America, while in the PI sequence, tree cover decreased in the region of present-day Peru. Furthermore, in the H1\_EXT sequence, trees increased in the Central Sahel, grasses increased markedly in a small region of Northwest Africa (Mauritania), while tree cover decreased regionally in the western tip of Senegal. A compilation of vegetation records from Western Equatorial Africa (Hessler et al., 2010) shows a reduction of forest biomes between 18.5 and 14.7 ka BP as well as at the end of the deglacial

## Climate and vegetation changes around the Atlantic Ocean

D. Handiani et al.

[Title Page](#)[Abstract](#)[Introduction](#)[Conclusions](#)[References](#)[Tables](#)[Figures](#)[⏪](#)[⏩](#)[◀](#)[▶](#)[Back](#)[Close](#)[Full Screen / Esc](#)[Printer-friendly Version](#)[Interactive Discussion](#)



## Climate and vegetation changes around the Atlantic Ocean

D. Handiani et al.

Title Page

Abstract

Introduction

Conclusions

References

Tables

Figures

⏪

⏩

◀

▶

Back

Close

Full Screen / Esc

Printer-friendly Version

Interactive Discussion



In our simulations with the UVic ESCM, the changes in northern tropical Africa were induced by a northward shift of the region of high precipitation (corresponding to the ITCZ) during abrupt warming resulting from the recovery of the AMOC. This complements studies (e.g. Kageyama et al., 2010; Swingedouw et al., 2009; Handiani et al., 2012) that have investigated the sensitivity of the tropical African vegetation to a southward shift of the ITCZ during abrupt cooling, e.g., at the onset of a Heinrich event.

We compared the vegetation patterns of two warmer climate phases: the pattern before the collapse of the AMOC (Heinrich event 1-like conditions, time  $T_{-1}$ ) with that at the end of sequence (after AMOC recovery, time  $T_2$ ). The comparison is intended to show similarities and differences of the vegetation cover during these two warmer climates. We found the vegetation patterns of the two climates state (PI and H1\_EXT) to be very similar. Differences in tree and grass cover were less than 10% and only occurred in a few areas, mostly around the North Atlantic Ocean. This finding may be compared to the hypothesis by Aitken et al. (2008) who propose that plant species respond to rapid climate change in three different ways: they either become extinct, persist in situ, or migrate to more suitable habitats. Our model results would be consistent with the second and third way, that is, persistence in situ or migration to more suitable habitats. Moreover, the total terrestrial carbon storage was nearly conserved in each sequence. The values before the abrupt cooling and at the end of the PI and H1\_EXT simulation sequences differed by about 10 gigatons of carbon (GtC) and 11 GtC, respectively. The corresponding relative changes were 0.5% and 0.8%, respectively.

## 5 Conclusions

Our simulations confirmed that under present-day climate conditions the addition of freshwater (in amounts comparable to meltwater pulse 1A) to the Southern Ocean may lead to a recovery of the AMOC after collapse (Weaver et al., 2003). However, under glacial climate conditions the AMOC behaved differently. With LGM-type initial

conditions the AMOC remained in a collapsed state, while with HE1-type initial conditions, the AMOC first slightly increased only to collapse again after freshwater hosing stopped. The North Atlantic Ocean warmed in response to adding freshwater to the Southern Ocean. It appears that in our model the AMOC is less sensitive to freshwater input to the Southern Ocean under glacial climate conditions than under present-day climate conditions. The AMOC did recover under glacial conditions when we extracted freshwater from the North Atlantic, mimicking a reduction of iceberg calving into the North Atlantic Ocean.

The impact of an intensifying AMOC and warming climate in the North Atlantic Ocean on vegetation patterns depended on background climatic conditions, although tropical Northern Africa was clearly the most sensitive area in terms of precipitation. With respect to vegetation changes during the BA period, in our model the zone of intense tropical precipitation shifted northward, followed by immediate and considerable vegetation changes, mostly in Northern tropical and subtropical Africa. Comparison with pollen compilation records from North America and Europe showed reasonable agreement.

The vegetation patterns before the AMOC collapsed and after it recovered were very similar. Changes in tree and grass cover were smaller than 10% and limited to a few areas around the North Atlantic Ocean, and the total terrestrial carbon storage was largely conserved. This transient nature of the simulated vegetation change is consistent with the hypothesis that vegetation cover persisted in situ or migrated to more appropriate habitats in response to abrupt climate change.

*Acknowledgements.* This work was funded by the Deutsche Forschungsgemeinschaft (DFG) as part of the German contribution to the Integrated Ocean Drilling Program (SPP 527) “Abrupt Climate Change in the African Tropics (ACCAT)” and the DFG Research Center/Excellence Cluster “The Ocean in the Earth System”. A part of financial support during the final production in this study was also given by “The Excellent Scholarship Program by Bureau of Planning and International Cooperation”, Secretary-General of Ministry of Education and Culture, Indonesia. The authors are grateful to the Climate Modelling Group at the University of Victoria for providing the UVic ESCM.

## Climate and vegetation changes around the Atlantic Ocean

D. Handiani et al.

Title Page

Abstract

Introduction

Conclusions

References

Tables

Figures



Back

Close

Full Screen / Esc

Printer-friendly Version

Interactive Discussion



## References

- Aitken, S. N., Yeaman, S. H., Holliday, J. A., Wang, T., and Curtis-McLane, S.: Adaptation, migration or extirpation: climate change outcomes for tree populations, *Evol. Appl.*, 1, 95–111, 2008.
- 5 Bard, E., Hamelin, B., and Fairbanks, R. G.: U/Th ages obtained by mass spectrometry in corals from Barbados: sea level during the past 130 000 years, *Nature*, 346, 456–458, 1990.
- Bard, E., Raisbeck, G. M., Yiou, F., and Jouzel, J.: Solar irradiance during the last 1200 years based on cosmogenic nuclides, *Tellus B*, 52, 985–992, 2000.
- Bard, E., Hamelin, B., and Delanghe-Sabatier, D.: Deglacial meltwater pulse 1B and Younger  
10 Dryas sea levels revisited with boreholes at Tahiti, *Science*, 327, 1235–1237, 2010.
- Barker, S., Diz, P., Vautravers, M. J., Pike, J., Knorr, G., Hall, I. R., and Broecker, W. S.: Inter-hemispheric Atlantic seesaw response during the last deglaciation, *Nature*, 457, 1097–1101, 2009.
- Bitz, C. M., Holland, M., Weaver, A. J., and Eby, M.: Simulating the ice-thickness distribution in  
15 a coupled climate model, *J. Geophys. Res.*, 106, 2441–2464, 2001.
- Boyle, E. A. and Keigwin, L. D.: North Atlantic thermohaline circulation during the last 20 000 years: link to high latitude surface temperature, *Nature*, 330, 35–40, 1987.
- Broecker, W. S.: Paleocean circulation during the last deglaciation: A bipolar seesaw?, *Paleoceanography*, 13, 119–121, 1998.
- 20 Clark, P. U., Alley, R. B., Keigwin, L. D., Licciardi, J. M., Johnsen, S. J., and Wang, H.: Origin of the first global meltwater pulse following the last glacial maximum, *Paleoceanography*, 11, 563–577, 1996.
- Clark, P. U., Mitrovica, J. X., Milne, G. A., and Tamisiea, M. E.: Sea-level fingerprinting as a direct test for the source of global meltwater pulse 1A, *Science*, 295, 2438–2441, doi:10.1126/Science.1068797, 2002.
- 25 Cox, P. M.: Description of the “TRIFFID” dynamic global vegetation model, Hadley Centre Technical Note 24, Met Office, Bracknell, 2001.
- Cox, P. M., Betts, R. A., Bunton, C. B., Essery, R. L. H., Rowntree, P. R., and Smith, J.: The impact of new land surface physics on the GCM simulation of climate and climate sensitivity,  
30 *Clim. Dynam.*, 15, 183–203, 1999.

### Climate and vegetation changes around the Atlantic Ocean

D. Handiani et al.

Title Page

Abstract

Introduction

Conclusions

References

Tables

Figures

⏪

⏩

◀

▶

Back

Close

Full Screen / Esc

Printer-friendly Version

Interactive Discussion



## Climate and vegetation changes around the Atlantic Ocean

D. Handiani et al.

[Title Page](#)
[Abstract](#)
[Introduction](#)
[Conclusions](#)
[References](#)
[Tables](#)
[Figures](#)




[Back](#)
[Close](#)
[Full Screen / Esc](#)
[Printer-friendly Version](#)
[Interactive Discussion](#)


- De Vries, P. and Weber, S. L.: The Atlantic freshwater budget as a diagnostic for the existence of a stable shut down of the meridional overturning circulation, *Geophys. Res. Lett.*, 32, L09606, doi:10.1029/2004GL021450, 2005.
- 5 Driesschaert, E., Fichefet, T., Goosse, H., Huybrechts, P., Janssens, I., Mouchet, A., Munhoven, G., Brovkin, V., and Weber, S. L.: Modeling the influence of Greenland ice sheet melting on the Atlantic meridional overturning circulation during the next millennia, *Geophys. Res. Lett.*, 34, L10707, doi:10.1029/2007GL029516, 2007.
- EPICA Community Members: One-to-one coupling of glacial climate variability in Greenland and Antarctica, *Nature*, 444, 195–198, doi:10.1038/nature05301, 2006.
- 10 Ewen, T. L., Weaver A. J., and Schmittner, A.: Modelling carbon cycle feedbacks during abrupt climate change, *Quaternary Sci. Rev.*, 23, 431–448, 2004.
- Fairbanks, R. G.: A 17 000 year glacio-eustatic sea level record: influence of glacial melting rates on the Younger Dryas event and deep ocean circulation, *Nature*, 342, 637–642, 1989.
- Fanning, A. F. and Weaver, A. J.: An atmospheric energy moisture-balance model: climatology, interpentadal climate change and coupling to an OGCM, *J. Geophys. Res.*, 101, 15111–15128, 1996.
- 15 Fletcher, W. J., Sanchez Goñi, M. F., Allen, J. R. M., Cheddadi, R., Combourieu Nebout, N., Huntley, B., Lawson, I., Londeix, L., Magri, D., Margari, V., Müller, U., Naughton, F., Novenko, E., Roucoux, K., and Tzedakis, P. C.: Millennial-scale variability during the last glacial in vegetation records from Europe, *Quaternary Sci. Rev.*, 29, 2839–2864, 2010.
- Ganopolski, A. and Rahmstorf, S.: Rapid changes of glacial climate simulated in a coupled climate model, *Nature*, 409, 153–158, doi:10.1038/35051500, 2001.
- Handiani, D., Paul, A., and Dupont, L.: Tropical climate and vegetation changes during Heinrich Event 1: a model-data comparison, *Clim. Past*, 8, 37–57, doi:10.5194/cp-8-37-2012, 2012.
- 25 Hessler I., Dupont, L. M., Bonnefille, R., Behling, H., González, C., Helmens, K. F., Hooghiemstra, H., Lebamba, J., Ledru, M.-P., Lézine, A.-M., Maley, J., Marret, F., and Vincens, A.: Millennial-scale changes in vegetation records from tropical Africa and South America during the last glacial, *Quaternary Sci. Rev.*, 29, 2882–2899, 2010.
- Hibler, W. D.: A dynamic thermodynamic sea ice model, *J. Phys. Oceanogr.*, 9, 815–846, 1979.
- 30 Hughes, T. M. C. and Weaver, A. J.: Multiple equilibria of an asymmetric two-basin ocean model, *J. Phys. Oceanogr.*, 24, 619–637, 1994.
- Hunke, E. C. and Dukowicz, J. K.: An elastic-viscous-plastic model for sea ice dynamics, *J. Phys. Oceanogr.*, 27, 1849–1867, 1997.

## Climate and vegetation changes around the Atlantic Ocean

D. Handiani et al.

Title Page

Abstract

Introduction

Conclusions

References

Tables

Figures



Back

Close

Full Screen / Esc

Printer-friendly Version

Interactive Discussion



Jiménez-Moreno, G., Anderson, R. S., Desprat, S., Grigg, L., Grimm, E., Heusser, L. E., Jacobs, B. F., López-Martínez, C., Whitlock, C., and Willard, D. A.: Millennial-scale variability during the last glacial in vegetation records from North America, *Quaternary Sci. Rev.*, 29, 2865–2881, 2010.

5 Kageyama, M., Mignot, J., Swingedouw, D., Marzin, C., Alkama, R., and Marti, O.: Glacial climate sensitivity to different states of the Atlantic Meridional Overturning Circulation: results from the IPSL model, *Clim. Past*, 5, 551–570, doi:10.5194/cp-5-551-2009, 2009.

Kageyama, M., Paul, A., Roche, D. M., and Van Meerbeeck, C. J.: Modelling glacial climatic millennial-scale variability related to changes in the Atlantic meridional overturning circulation: a review, *Quaternary Sci. Rev.*, 29, 2931–2956, 2010.

10 Kanfoush, S. L., Hodell, D. A., Charles, C. D., Guilderson, T. P., Mortyn, P. G., and Ninne-  
mann, U. S.: Millennial-scale instability of the Antarctic ice sheet during the last glaciation, *Science*, 288, 1815–1818, 2000.

Knorr, G. and Lohmann, G.: Rapid transitions in the Atlantic thermohaline circulation triggered by global warming and meltwater during the last deglaciation, *Geochem. Geophys. Geosy.*, 8, Q12006, doi:10.1029/2007GC001604, 2007.

15 Liu, Z., Otto-Bliesner, B. L., He, F., Brady, E. C., Tomas, R., Clark, P. U., Carlson, A. E., Lynch-Stieglitz, J., Curry, W., Brook, E., Erickson, D., Jacob, R., Kutzbach, J., and Cheng, J.: Transient simulation of last deglaciation with a new mechanism for Bølling-Allerød warming, *Science*, 325, 310–314, 2009.

Manabe, S. and Stouffer, R. J.: Coupled ocean-atmosphere model response to freshwater input: comparison to Younger Dryas event, *Paleoceanography*, 12, 321–336, 1997.

Matthews, H. D., Weaver, A. J., and Meissner, K. J.: Terrestrial carbon cycle dynamics under recent and future climate change, *J. Climate*, 18, 1609–1628, 2005.

25 McManus, J. F., Francois, R., Gherardi, J.-M., Keigwin, L. D., and Brown-Leger, S.: Collapse and rapid resumption of Atlantic meridional circulation linked to deglacial climate changes, *Nature*, 428, 834–837, 2004.

Meissner, K. J., Weaver, A. J., Matthews, H. D., and Cox, P. M.: The role of land surface dynamics in glacial inception: A study with the UVic Earth System model, *Clim. Dynam.*, 21, 515–537, 2003.

30 Pacanowski, R. C.: MOM 2 documentation: Users guide and reference manual, Version 1.0. GFDL Ocean Group Technical Report No. 3, Geophysical Fluid Dynamics Laboratory, Princeton, New Jersey, 1995.

---

## Climate and vegetation changes around the Atlantic Ocean

D. Handiani et al.

---

Title Page

Abstract

Introduction

Conclusions

References

Tables

Figures

◀

▶

◀

▶

Back

Close

Full Screen / Esc

Printer-friendly Version

Interactive Discussion



- Peltier, W. R.: Global glacial isostasy and the surface of the ice-age earth: the ICE-5G (VM2) model and GRACE, *Annu. Rev. Earth Pl. Sc.*, 32, 111–149, 2004.
- Peltier, W. R., Vettoretti, G., and Stastna, M.: Atlantic meridional overturning and climate response to Arctic ocean freshening, *Geophys. Res. Lett.*, 33, L06713, doi:10.1029/2005GL025251, 2006.
- Schmittner, A., Meissner, K. J., Eby, M., and Weaver, A. J.: Forcing of the deep ocean circulation in simulations of the last glacial maximum, *Paleoceanography*, 17, 1015, doi:10.1029/2001PA000633, 2002a.
- Schmittner, A., Yoshimori, M., and Weaver, A. J.: Instability of glacial climate in a model of the ocean-atmosphere-cryosphere system, *Science*, 295, 1489–1493, 2002b.
- Schmittner, A., Brook, E., and Ahn, J.: Impact of the ocean's overturning circulation on atmospheric CO<sub>2</sub> in Ocean Circulation: mechanisms and impacts, AGU Geophysical Monograph Series, Vol. 173, edited by: Schmittner, A., Chiang, J., and Hemming, S., 209–246, 2007.
- Siddall, M., Smeed, D. A., Hemleben, C., Rohling, E. J., Schmelzer, I., and Peltier, W. R.: Understanding the Red Sea response to sea level, *Earth Planet. Sc. Lett.*, 225, 421–434, doi:10.1016/j.epsl.2004.06.008, 2004.
- Stanford, J. D., Rohling, E. J., Hunter, S. E., Roberts, A. P., Rasmussen, S. O., Bard, E., McManus, J., and Fairbanks, R. G.: Timing of meltwater pulse 1a and climate responses to meltwater injections, *Paleoceanography*, 21, PA4103, doi:10.1029/2006PA001340, 2006.
- Stenni, B., Burion, D., Frezzotti, M., Albani, S., Barbante, C., Bard, E., Barnola, J. M., Baroni, M., Baumgartner, M., Bonazza, M., Capron, E., Castellano, E., Chappellaz, J., Delmonte, B., Falourd, S., Genoni, L., Iacumin, P., Jouzel, J., Kipfstuhl, S., Landais, A., Lemieux-Dudon, B., Maggi, V., Masson-Delmotte, V., Mazzola, C., Minster, B., Montagnat, M., Mulvaney, R., Narcisi, B., Oerter, H., Parrenin, F., Petit, J. R., Ritz, C., Scarchilli, C., Schilt, A., Schüpbach, S., Schwander, J., Selmo, E., Severi, M., Stocker, T. F., and Udisti, R.: Expression of the bipolar see-saw in Antarctic climate records during the last deglaciation, *Nat. Geosci.*, 4, 46–49, 2011.
- Stocker, T. F. and Johnsen, S. J.: A minimum model for the bipolar seesaw, *Paleoceanography*, 18, 1087, doi:10.1029/2003PA000920, 2003.
- Stocker, T. F. and Wright, D. G.: The effect of a succession of ocean ventilation changes on radiocarbon, *Radiocarbon*, 40, 359–366, 1998.
- Stocker, T. F., Wright, D. G., and Broecker, W. S.: Influence of high-latitude surface forcing on the global thermohaline circulation, *Paleoceanography*, 7, 529–541, 1992.

## Climate and vegetation changes around the Atlantic Ocean

D. Handiani et al.

Title Page

Abstract

Introduction

Conclusions

References

Tables

Figures

◀

▶

◀

▶

Back

Close

Full Screen / Esc

Printer-friendly Version

Interactive Discussion



Stocker, T. F., Knutti, R., and Plattner, G.-K.: The Future of the Thermohaline Circulation – A Perspective, in: *The Oceans and Rapid Climate Change: Past, Present, and Future*, edited by: Seidov, D., Maslin, M., and Haupt, B. J., Vol. 126 of *Geophysical Monograph*, 277–293, Am. Geophys. Union, Washington, DC, 2001.

5 Stouffer, R. J., Seidov, D., and Haupt, B. J.: Climate response to external sources of freshwater: North Atlantic versus the Southern Ocean, *J. Climate*, 20, 436–448, 2006.

Swingedouw, D., Mignot, L. J., Braconnot, P., Mosquet, E., Kageyama, M., and Alkama, R.: Impact of freshwater release in the North Atlantic under different climate conditions in an OAGCM, *J. Climate*, 22, 6377–6401, 2009.

10 Trevena, J., Sijp, W. P., and England, M. H.: North Atlantic deep water collapse triggered by a Southern Ocean meltwater pulse in a glacial climate state, *Geophys. Res. Lett.*, 35, L09704, doi:10.1029/2008GL033236, 2008.

Weaver, A. J., Eby, M., Wiebe, E. C., Bitz, C. M., Duffy, P. B., Ewen, T. L., Fanning, A. F., Holland, M. M., MacFadyen, A., Matthews, H. D., Meissner, K. J., Saenko, O., Schmittner, A., Wang, H., and Yoshimori, M.: The UVic Earth System Climate Model: model description, climatology, and applications to past, present and future climates, *Atmos. Ocean*, 39, 361–428, 2001.

Weaver, A. J., Saenko, O. A., Clark, P. U., and Mitrovica, J. X.: Meltwater pulse 1A from Antarctica as a trigger of the Bølling-Allerød warm interval, *Science*, 299, 1709–1713, 2003.

20 Weaver, A. J., Eby, M., Kienast, M., and Saenko, O. A.: Response of the Atlantic meridional overturning circulation to increasing atmospheric CO<sub>2</sub>: sensitivity to mean climate state, *Geophys. Res. Lett.*, 34, L05708, doi:10.1029/2006GL028756, 2007.

Weber, S. L. and Drijfhout, S. S.: Stability of the Atlantic meridional overturning circulation in the Last Glacial maximum climate, *Geophys. Res. Lett.*, 34, L22706, doi:10.1029/2007GL031437, 2007.

25 Weber, S. L., Drijfhout, S. S., Abe-Ouchi, A., Crucifix, M., Eby, M., Ganopolski, A., Murakami, S., Otto-Bliesner, B., and Peltier, W. R.: The modern and glacial overturning circulation in the Atlantic ocean in PMIP coupled model simulations, *Clim. Past*, 3, 51–64, doi:10.5194/cp-3-51-2007, 2007.

30 Wiebe, E. C. and Weaver, A. J.: On the sensitivity of global warming experiments to the parametrisation of sub-grid scale ocean mixing, *Clim. Dynam.*, 15, 875–893, 1999.

## Climate and vegetation changes around the Atlantic Ocean

D. Handiani et al.

**Table 1.** Experimental design and boundary conditions as well as hosing locations (denoted in Fig. 1a).

Experiment	Boundary conditions		The HE1 freshwater hosing experiment			The BA freshwater hosing experiment		
	Insolation	CO <sub>2</sub> (ppm)	Rates (Sv)	Hosing location	Years simulation	Rates (Sv)	Hosing location	Years simulation
PI	1950	310	0–0.2	A	1000	0–1.0	B	500
GL	21 ka	200	0–0.2	A	1000	0–1.0	B	500
H1	16 ka	220	0–0.2	A	1000	0–1.0	B	500
H1_EXT	16 ka	220	0–0.2	A	1000	–0.3	C	500

[Title Page](#)
[Abstract](#)
[Introduction](#)
[Conclusions](#)
[References](#)
[Tables](#)
[Figures](#)
[Back](#)
[Close](#)
[Full Screen / Esc](#)
[Printer-friendly Version](#)
[Interactive Discussion](#)


## Climate and vegetation changes around the Atlantic Ocean

D. Handiani et al.

[Title Page](#)
[Abstract](#)
[Introduction](#)
[Conclusions](#)
[References](#)
[Tables](#)
[Figures](#)
[Back](#)
[Close](#)
[Full Screen / Esc](#)
[Printer-friendly Version](#)
[Interactive Discussion](#)

**Table 2.** The pollen records used in the biome reconstruction for the BA period compiled for the terrestrial regions around the Atlantic Ocean (Europe, North America, tropical South America and Africa) (see also Fig. 1a, b).

ID No.	Latitude and Longitude	Sites	Biomes reconstruction
North America sites (reference: Jiménez-Moreno et al., 2010)			
1.	45.91° N; 120.88° W	Carp Lake	Tundra
2.	42.23° N; 125.81° W	EW-9504-17PC	Temperate forest
3.	34.28° N; 120.03° W	ODP 893A	Temperate forest
4.	32.90° N; 119.73° W	F2-92-P29	Warm-temperate forest
5.	35.38° N; 111.71° W	Walker Lake	Grassland and dry shrubland
6.	34.45° N; 111.33° W	Potato Lake	Boreal forest
7.	30.26° N; 85.01° W	Camel Lake	Temperate forest
Europe sites (reference: Fletcher et al., 2010)			
8.	36.20° N; 4.30° E	ODP site 976	Temperate forest
9.	36.13° N; 2.62° E	MD95-2043	Temperate forest
10.	40.58° N; 10.35° E	MD95-2039	Grassland and dry shrubland
11.	41.15° N; 9.68° E	MD99-2331 (MD03-2697)	Temperate forest
12.	40.93° N; 15.62° W	Lago Grande di Monticchio	Temperate forest
13.	41.88° N; 12.77° W	Valle di Castiglione	Grassland and dry shrubland
14.	42.57° N; 11.80° W	Lagaccione	Temperate forest
Equatorial Africa (reference: Hessler et al., 2010)			
15.	3.47° S; 29.57° E	Kashiru Bog, Burundi	Savannah and xerophytic scrubland
16.	9.33° S; 33.75° E	Lake Masoko, Tanzania	Warm temperate mixed forest
Equatorial South America (reference: Hessler et al., 2010)			
17.	23.87° S; 46.71° W	Colônia, Brazil	Savannah and xerophytic scrubland
18.	5.45° N; 73.46° W	Fúquene, Colombia	Warm temperate mixed forest
19.	3.67° S; 37.72° W	GeoB 3104 – off NE Brazil	Warm temperate mixed forest

## Climate and vegetation changes around the Atlantic Ocean

D. Handiani et al.

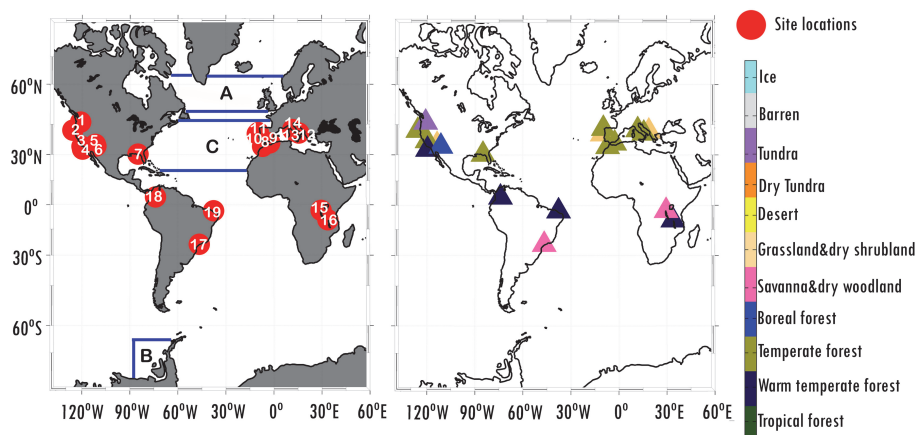


**Fig. 1.** (a) Location sites of pollen records mentioned in Table 2 and the freshwater discharge locations: east of the St. Lawrence River (region A), west of West Antarctica (region B), the North Atlantic Ocean between latitude of 20° N–50° N (negative discharge in region C). (b) The biomes reconstruction during the onset of BA (see Table 2).

Title Page

Abstract

Introduction

Conclusions

References

Tables

Figures

◀

▶

◀

▶

Back

Close

Full Screen / Esc

Printer-friendly Version

Interactive Discussion

## Climate and vegetation changes around the Atlantic Ocean

D. Handiani et al.

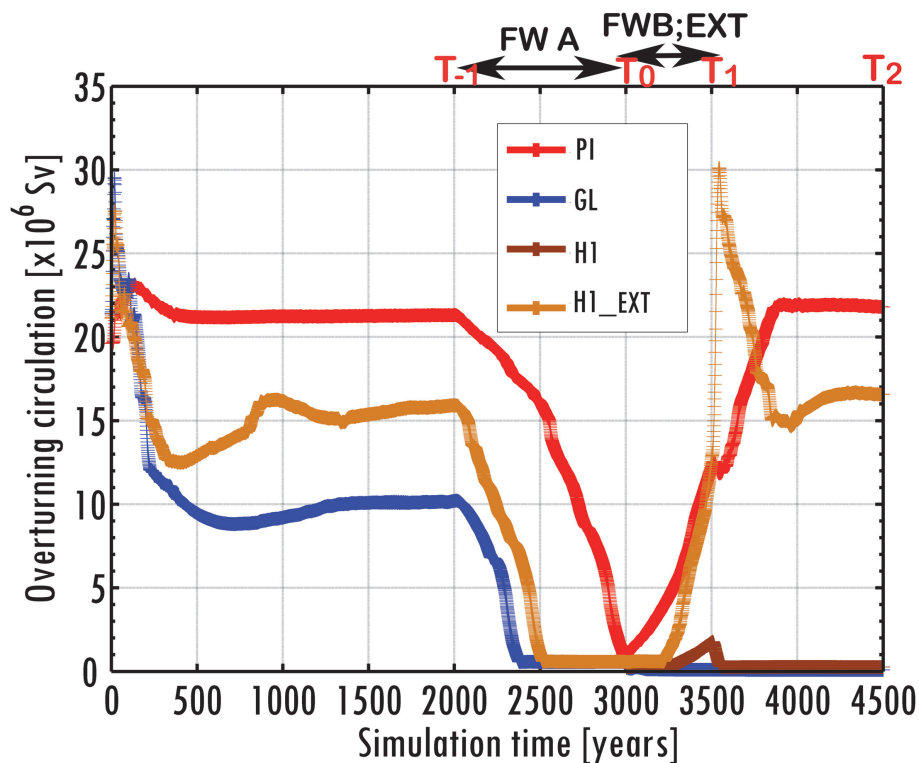


**Fig. 2.** The AMOC streamfunction maximum for all sequences (see for experimental setup Table 1). Anomaly plots in the following figures have been calculated between simulation times  $T_1$  and  $T_0$ .

Title Page

Abstract

Introduction

Conclusions

References

Tables

Figures

◀

▶

◀

▶

Back

Close

Full Screen / Esc

Printer-friendly Version

Interactive Discussion

# Climate and vegetation changes around the Atlantic Ocean

D. Handiani et al.

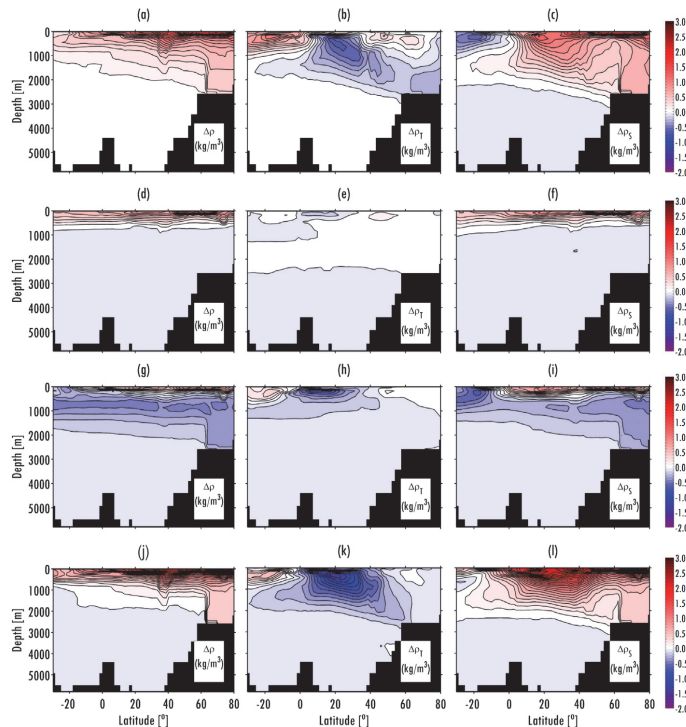


**Fig. 3.** Annual-mean anomaly density plots showing differences between time  $T_1$ , after 500 years of adding freshwater in region B, and time  $T_0$ , at the end of the freshwater perturbation at region A, for sequences PI (a–c), GL (d–f), H1 (g–i), and H1\_EXT (j–l); for each sequence the plots are decomposed into contributions from temperature changes  $\Delta\rho_T$  (b, e, h, k) and salinity changes  $\Delta\rho_S$  (c, f, i, l). The isoline differences for each plot are  $0.1 \text{ kg m}^{-3}$ .

## Climate and vegetation changes around the Atlantic Ocean

D. Handiani et al.

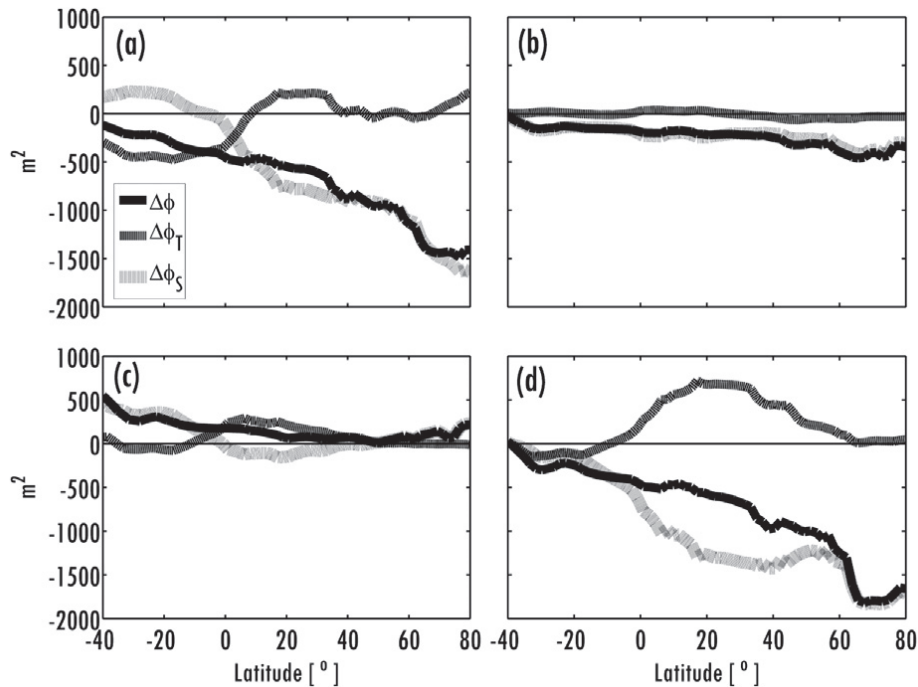


**Fig. 4.** Same as Fig. 3 but for annual zonally averaged depth-integrated steric height for sequences (a) PI, (b) GL, (c) H1, and (d) H1\_EXT. The total differences in steric height ( $\Delta\phi$ ) is a combination of temperature ( $\Delta\phi_T$ ) and salinity changes ( $\Delta\phi_S$ ).

Title Page

Abstract

Introduction

Conclusions

References

Tables

Figures

◀

▶

◀

▶

Back

Close

Full Screen / Esc

Printer-friendly Version

Interactive Discussion

## Climate and vegetation changes around the Atlantic Ocean

D. Handiani et al.

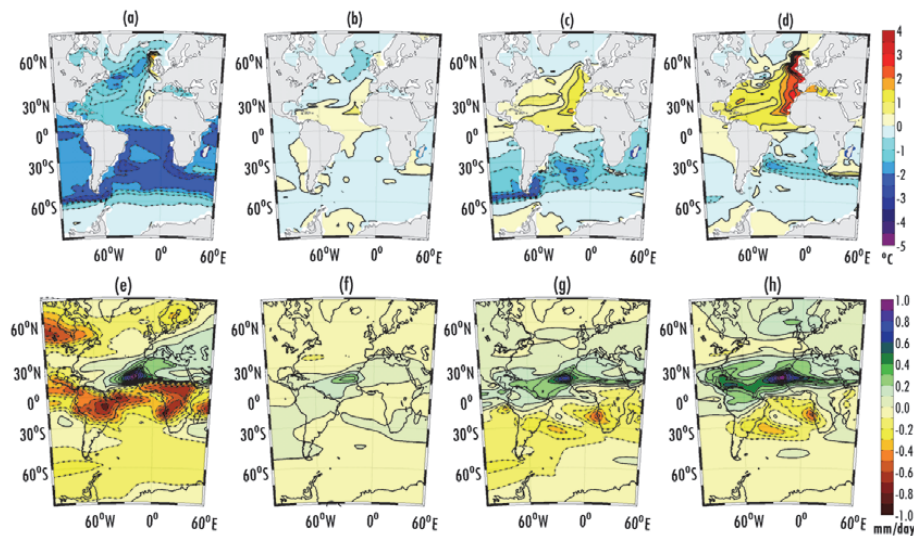


**Fig. 5.** Same as Fig. 3 but for annual mean anomaly of sea surface temperature (SST, top panel) and precipitation (bottom panel) for sequences PI (a, e), GL (b, f), H1 (c, g), and H1\_EXT (d, h).

Title Page

Abstract

Introduction

Conclusions

References

Tables

Figures

◀

▶

◀

▶

Back

Close

Full Screen / Esc

Printer-friendly Version

Interactive Discussion

## Climate and vegetation changes around the Atlantic Ocean

D. Handiani et al.

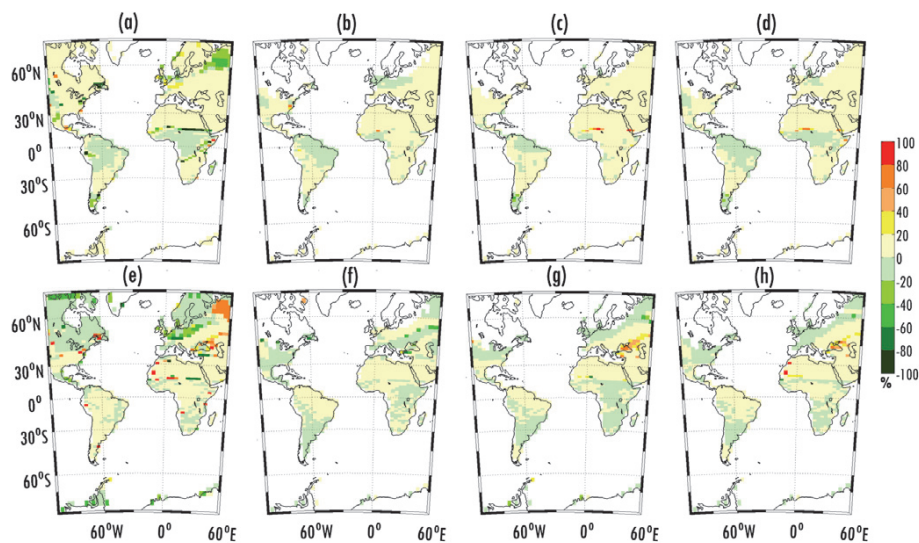


**Fig. 6.** Same as Fig. 3 but for annual mean anomaly of tree cover (**a–d**) and grass cover (**e–h**) for sequences PI (**a, e**), GL (**b, f**), H1 (**c, g**), and H1\_EXT (**d, h**).

[Title Page](#)[Abstract](#)[Introduction](#)[Conclusions](#)[References](#)[Tables](#)[Figures](#)[◀](#)[▶](#)[◀](#)[▶](#)[Back](#)[Close](#)[Full Screen / Esc](#)[Printer-friendly Version](#)[Interactive Discussion](#)

Climate and  
vegetation changes  
around the Atlantic  
Ocean

D. Handiani et al.

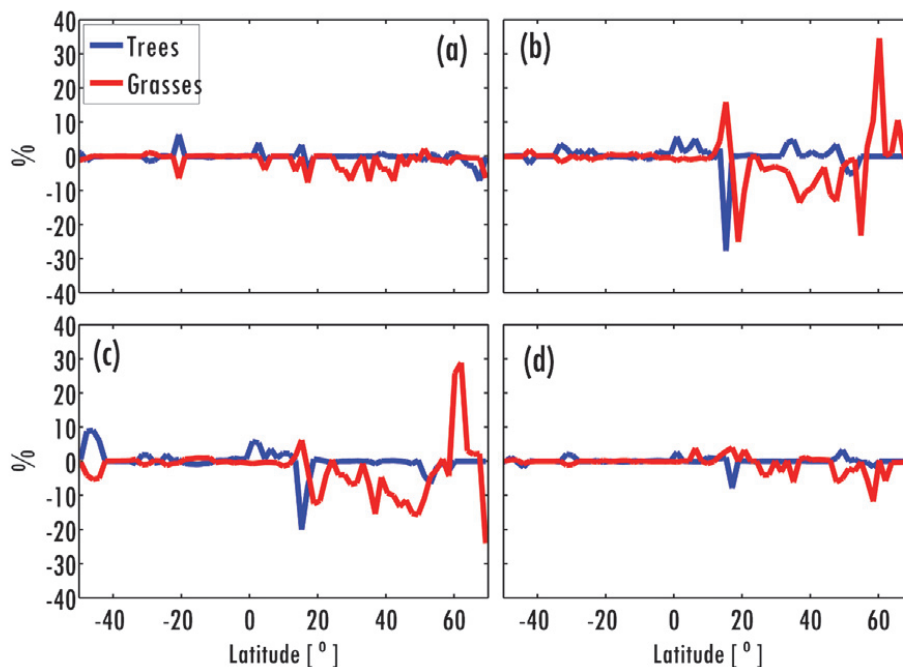


**Fig. 7.** Annual anomaly of zonally averaged tree and grass cover showing differences between time  $T_2$ , at the end of sequence (see Fig. 2), and time  $T_{-1}$ , before adding freshwater to region A, for sequences PI (a), GL (b), H1 (c), and H1\_EXT (d) in the area between 110° W to 60° E and 50° S to 70° N.

Title Page

Abstract

Introduction

Conclusions

References

Tables

Figures

◀

▶

◀

▶

Back

Close

Full Screen / Esc

Printer-friendly Version

Interactive Discussion

## Climate and vegetation changes around the Atlantic Ocean

D. Handiani et al.

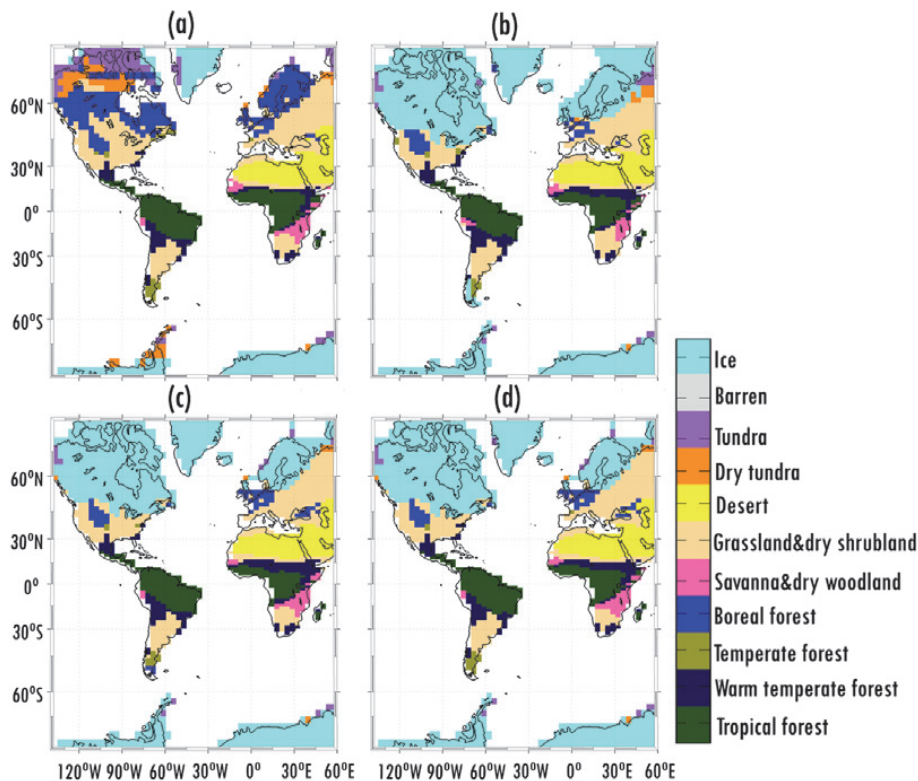


**Fig. 8.** Biome distribution at time  $T_1$ , after 500 years of adding freshwater in region B, calculated after a simply algorithm (Handiani et al., 2012) combining the potential PFTs and the environmental limitations from the model output for sequences (a) PI, (b) GL, (c) H1, and (d) H1\_EXT. The simulated biomes were compiled into mega-biomes as defined by Harrison and Prentice (2003).

Title Page

Abstract

Introduction

Conclusions

References

Tables

Figures

◀

▶

◀

▶

Back

Close

Full Screen / Esc

Printer-friendly Version

Interactive Discussion